

## Evidence for a pulsar wind nebula in the Type Ib-peculiar supernova SN 2012au

DAN MILISAVLJEVIC,<sup>1</sup> DANIEL J. PATNAUDE,<sup>2</sup> ROGER A. CHEVALIER,<sup>3</sup> JOHN C. RAYMOND,<sup>2</sup> ROBERT A. FESEN,<sup>4</sup>  
RAFFAELLA MARGUTTI,<sup>5</sup> BRODY CONNER,<sup>1</sup> AND JOHN BANOVETZ<sup>1</sup>

<sup>1</sup>*Department of Physics and Astronomy, Purdue University, 525 Northwestern Ave., West Lafayette, IN. 47907, USA*

<sup>2</sup>*Smithsonian Astrophysical Observatory, 60 Garden St., Cambridge, MA 02138, USA*

<sup>3</sup>*Department of Astronomy, University of Virginia, P.O. Box 400325, Charlottesville, VA 22904, USA*

<sup>4</sup>*6127 Wilder Laboratory, Department of Physics and Astronomy, Dartmouth College, Hanover, NH 03755, USA*

<sup>5</sup>*Center for Interdisciplinary Exploration and Research in Astrophysics (CIERA) and Department of Physics and Astronomy, Northwestern University, Evanston, IL 60208*

(Received August 1, 2018; Revised August 24, 2018; Accepted August 28, 2018)

Submitted to ApJL

### ABSTRACT

We present an optical spectrum of the energetic Type Ib supernova (SN) 2012au obtained at an unprecedented epoch of 6.2 years after explosion. Forbidden transition emission lines of oxygen and sulfur are detected with expansion velocities of  $\approx 2300 \text{ km s}^{-1}$ . The lack of narrow H Balmer lines suggests that interaction with circumstellar material is not a dominant source of the observed late-time emission. We also present a deep *Chandra* observation that reveals no X-ray emission down to a luminosity of  $L_X < 2 \times 10^{38} \text{ erg s}^{-1}$  (0.5–10 keV). Our findings are consistent with the notion that SN 2012au is associated with a diverse subset of SNe, including long-duration gamma-ray burst SNe and superluminous SNe, harboring pulsar/magnetar wind nebulae that influence core-collapse explosion dynamics on a wide range of energy scales. We hypothesize that these systems may all evolve into a similar late-time phase dominated by forbidden oxygen transitions, and predict that emission line widths should remain constant or broaden a few per cent per year due to the acceleration of ejecta by the pulsar/magnetar bubble.

*Keywords:* supernovae: general — supernovae: individual(SN 2012au) — pulsars: general — stars: magnetars

### 1. INTRODUCTION

Models of hydrogen-poor and energetic ( $E_k \sim 10^{52}$  erg) broad-lined Type Ic (Ic-bl) core-collapse supernovae (SNe) associated with long-duration gamma-ray bursts (GRBs) often invoke central engine-driven mechanisms associated with the formation of compact objects that input energy into the explosion. The “collapsar” mechanism (MacFadyen & Woosley 1999), which involves a massive star collapsing directly to a black hole with accretion releasing energy in the form of a relativistic jet that can explode the star, has long been a favored model (Woosley & Heger 2012). However, mounting evidence supports the view that these explosions may be pow-

ered by rapidly rotating “magnetars,” i.e., a neutron star with an exceptionally strong ( $> 10^{14}$  G) magnetic field (Thompson et al. 2004; Metzger et al. 2011; Mazzali et al. 2014; Metzger et al. 2015).

Magnetars have also been used in models characterizing the diverse class of hydrogen-poor superluminous SNe (SLSNe-I; Inserra et al. 2013; Nicholl et al. 2013). SLSNe-I can radiate more than  $10^{44} \text{ erg s}^{-1}$  at their peak luminosity and may be associated with extremely massive ( $> 100 M_\odot$ ) progenitor stars. Their slow-evolving light curves are consistent with those expected from the decay of tremendous amounts of radioactive  $^{56}\text{Ni}$  ( $> 3 M_\odot$ ), as might be synthesized by a pair-instability explosion. However, this scenario fails in numerous cases where the luminosity reaches levels requiring the nickel mass to be larger than the estimated ejecta mass.

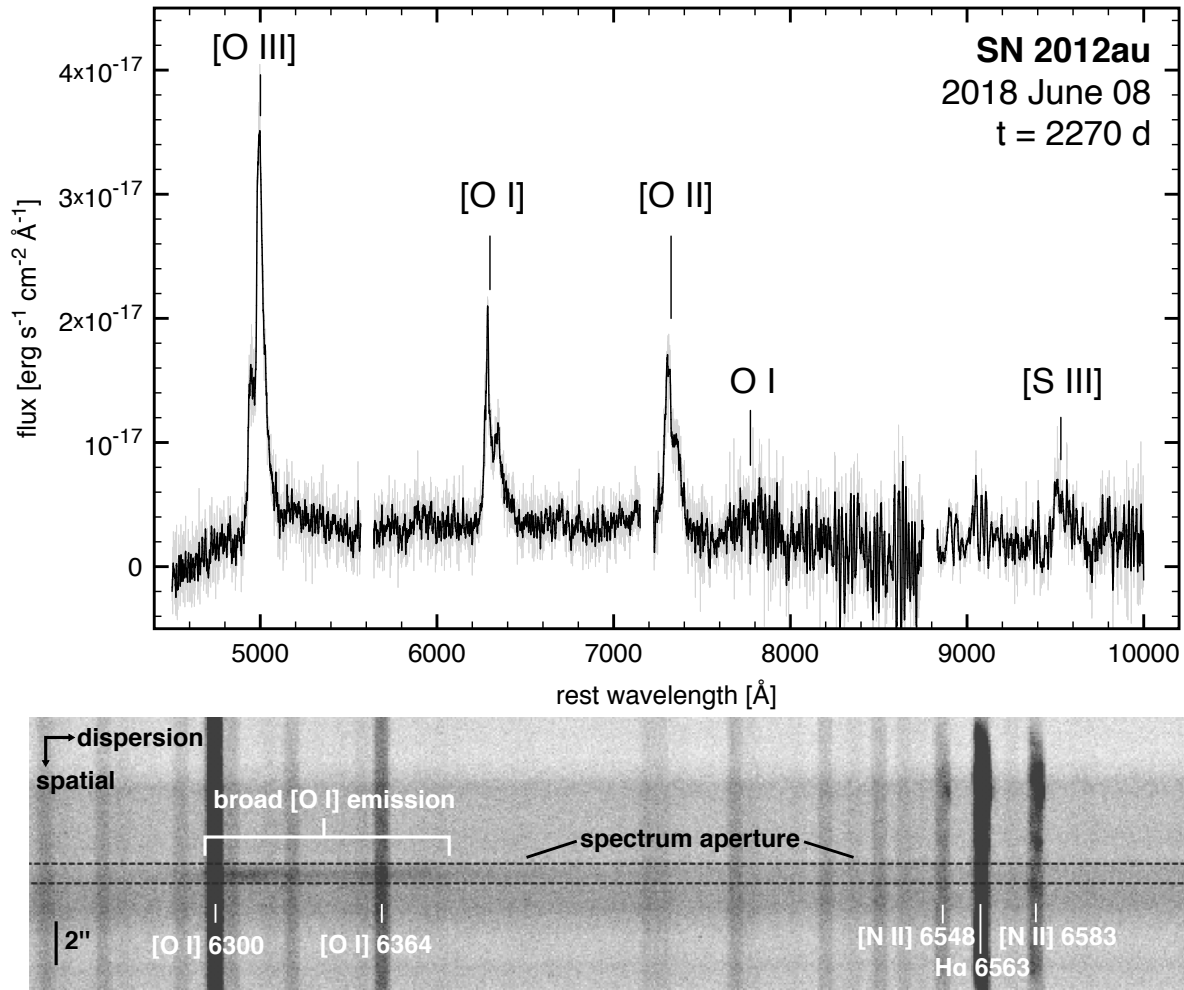


**Figure 1.** Magellan+IMACS optical spectrum of SN 2012au obtained 2018 June 8. *Top:* Entire 1D spectrum as extracted (gray) and data smoothed using 5 Å boxcar (black). The phase is with respect to the  $v$ -band maximum on 2012 March 21. *Bottom:* 2D spectrum in the region of [O I] and H $\alpha$ . No conspicuous narrow emission lines local to the SN are observed.

Interaction between a SLSN-I and surrounding circumstellar material (CSM) is another possible energy source (Chatzopoulos & Wheeler 2012). However, SLSN-I events generally lack conspicuous spectroscopic features that support this interpretation at photospheric stages. SLSN–CSM interaction also requires an extreme mass-loss history of several  $M_{\odot}$  of H-poor material shed in the last year before explosion in order to reproduce the observed light curves (Chevalier & Irwin 2011; Lunnan et al. 2018).

Discovery of SN 2011kl, which had a higher-than-average luminosity and was associated with the ultra-long-duration GRB 111209A, suggests that GRB and SLSN classifications are not necessarily distinct (Greiner et al. 2015). Understanding the SLSN–GRB connection is presently an area of active investigation (Pian & Mazzali 2017; Coppejans et al. 2018; Margutti et al. 2017). The connection was anticipated by earlier observations of the SLSN 2010gx (Pastorello et al. 2010), and the un-

usually energetic ( $E_k \sim 10^{52}$  erg), slow-evolving, Type Ib SN 2012au, which is believed to be a lower-luminosity counterpart to SLSNe (Milisavljevic et al. 2013; Kamble et al. 2014; Milisavljevic & Margutti 2018). Nebular phase observations of the SLSN 2015bn (Nicholl et al. 2016) and other SLSNe-I (Nicholl et al. 2018) have further strengthened the connection. Core angular momentum may be the key ingredient differentiating SLSNe and GRBs (Lunnan et al. 2014). However, other factors including star formation rate and stellar mass may also be influential (Angus et al. 2016). Recent speculation that Fast Radio Bursts (FRBs) may be magnetars in the remnants of SLSN explosions has heightened the significance of the SLSN–GRB connection (Metzger et al. 2017; Nicholl et al. 2017; Eftekhari et al. 2018).

Here we present optical and X-ray data of SN 2012au obtained  $> 6$  yr post-explosion that offer fresh insight into the suspected link between SLSNe and GRB-SNe. In sections 2 and 3 we present our optical spectroscopy

and supporting X-ray observations, along with analysis and results. In sections 4 and 5 we discuss possible excitation mechanisms and outline numerous arguments in favor of heating of ejecta by a pulsar wind nebula (PWN). Our discovery marks the first time a PWN signature has been detected in a verified extragalactic SN Ib at this extremely late epoch. We conclude in section 6 with implications of our result and suggest future avenues of investigation. We adopt  $23.5 \pm 0.5$  Mpc as the distance to the host galaxy NGC 4790 (Theureau et al. 2007).

## 2. OBSERVATIONS

### 2.1. Optical Spectroscopy

A low resolution optical spectrum of SN 2012au was obtained with the 6.5m Magellan telescope at Las Campanas Observatory on 2018 June 8. The Inamori Magellan Areal Camera and Spectrograph (IMACS; Dressler et al. 2011) was used with the f/4 camera in combination with the Mosaic3 array of eight thinned  $2\text{K} \times 4\text{K} \times 15\text{-}\mu\text{m}$  E2V CCDs. A 300 lines  $\text{mm}^{-1}$  grating and a  $0.9''$  long slit were used. Exposures of  $2 \times 3000$  sec were obtained and averaged. Resulting spectra have an effective wavelength range of 4520-10,000 Å, with dispersion of  $0.74 \text{ Å pixel}^{-1}$  and full-width-half-maximum (FWHM) resolution of 5 Å (measured at 6000 Å). The spectrum has interruptions in coverage between detector gaps. The seeing was  $0.6''$  and conditions were generally clear but not photometric.

Standard procedures to bias-correct, flat-field, and flux-calibrate the data were followed using IRAF. LA-Cosmic (van Dokkum 2001) was used to remove cosmic rays in individual images. Some cosmetic defects introduced from hot pixels and imperfect background subtraction have been manually removed. Spectrophotometric standards Feige 56 and LTT 3864 were observed and used for absolute flux calibration (Hamuy et al. 2002), which is believed to be accurate to within 30%. The spectrum has been corrected for the redshift  $z = 0.004483$  of NGC 4790 (Theureau et al. 2007).

### 2.2. Chandra X-ray Observations

We obtained a 20 ksec observation of SN 2012au with the *Chandra X-ray Observatory* (CXO) in combination with ACIS-S on 2018 August 2 through Director’s Discretionary Time (PI: Patnaude; Observation ID 21660). Data have been reduced with the CIAO software v4.10 and corresponding calibration files. In a  $2''$  radius region centered on the SN, we detect a count rate of  $(3 \pm 3.5) \times 10^{-4} \text{ ct s}^{-1}$  (0.5–10 keV), consistent with background. Thus, no X-rays are detected from SN 2012au. The neutral hydrogen column density in

**Table 1.** Line fluxes and luminosities

Line	Flux <sup>a</sup>	Luminosity <sup>b</sup>
[O III] $\lambda\lambda 4959, 5007$	$2.10 \pm 0.04$	$1.4 \pm 0.05$
[O I] $\lambda\lambda 6300, 6364$	$0.99 \pm 0.02$	$0.65 \pm 0.02$
[O II] $\lambda\lambda 7319, 7330$	$0.96 \pm 0.03$	$0.64 \pm 0.03$
O I $\lambda 7774$	$0.26 \pm 0.03$	$0.17 \pm 0.02$
[S III] $\lambda\lambda 9069, 9531$	$0.62 \pm 0.06^c$	$0.41 \pm 0.04$

<sup>a</sup>In units of  $10^{-15} \text{ erg s}^{-1} \text{ cm}^{-2}$

<sup>b</sup>In units of  $10^{38} \text{ erg s}^{-1}$

<sup>c</sup>Estimated from  $4/3 \times [\text{S III}] 9531$  line flux

the direction of SN 2012au is  $3.8 \times 10^{20} \text{ cm}^{-2}$  (Kalberla et al. 2005). For an assumed non-thermal spectrum with index  $\Gamma = 2$ , we derive an unabsorbed flux limit of  $2.8 \times 10^{-15} \text{ erg s}^{-1} \text{ cm}^{-2}$ , corresponding to luminosity  $L_X < 2 \times 10^{38} \text{ erg s}^{-1}$  (0.5 – 10 keV).

## 3. ANALYSIS AND RESULTS

### 3.1. Spectral Properties

In Figure 1, we present our day 2270 spectrum of SN 2012au. Forbidden oxygen transitions [O I]  $\lambda\lambda 6300, 6364$ , [O II]  $\lambda\lambda 7319, 7330$ , and [O III]  $\lambda\lambda 4959, 5007$  are clearly observed. The [S III]  $\lambda 9531$  line is also detected but its doublet line [S III]  $\lambda 9069$  that is intrinsically  $\approx 1/3$  the strength is not recovered from noise largely associated with the subtraction of telluric lines and fringing. Broad but weak emission centered around 7775 Å is also observed, which we identify with O I  $\lambda 7774$ . Emission line fluxes and luminosities are listed in Table 1.

All forbidden line profiles exhibit a clear asymmetry towards blueshifted wavelengths, peaking at  $-700 \pm 50 \text{ km s}^{-1}$  (Fig. 2). We measure the expansion velocity of [O III], [O I], [O II], and [S III] using the half-width-zero-intensity (HWZI) shortward of 4959 Å, 6300 Å, 7325 Å, and 9531 Å, respectively. All measurements extend to approximately  $2300 \pm 100 \text{ km s}^{-1}$ . The weakly detected O I 7774 has no clear peak in emission and does not appear to have the same emission line profile as the forbidden transitions.

Excess flux is observed between 5100-5400 Å. This could potentially be the remnant of the “plateau” of emission observed in the day 321 spectrum (Milisavljevic et al. 2013; Fig. 3). However, contaminating flux from the host galaxy cannot be ruled out. The fall-off in flux below 4800 Å is attributed to rapid loss of instrument sensitivity at these shorter wavelengths.

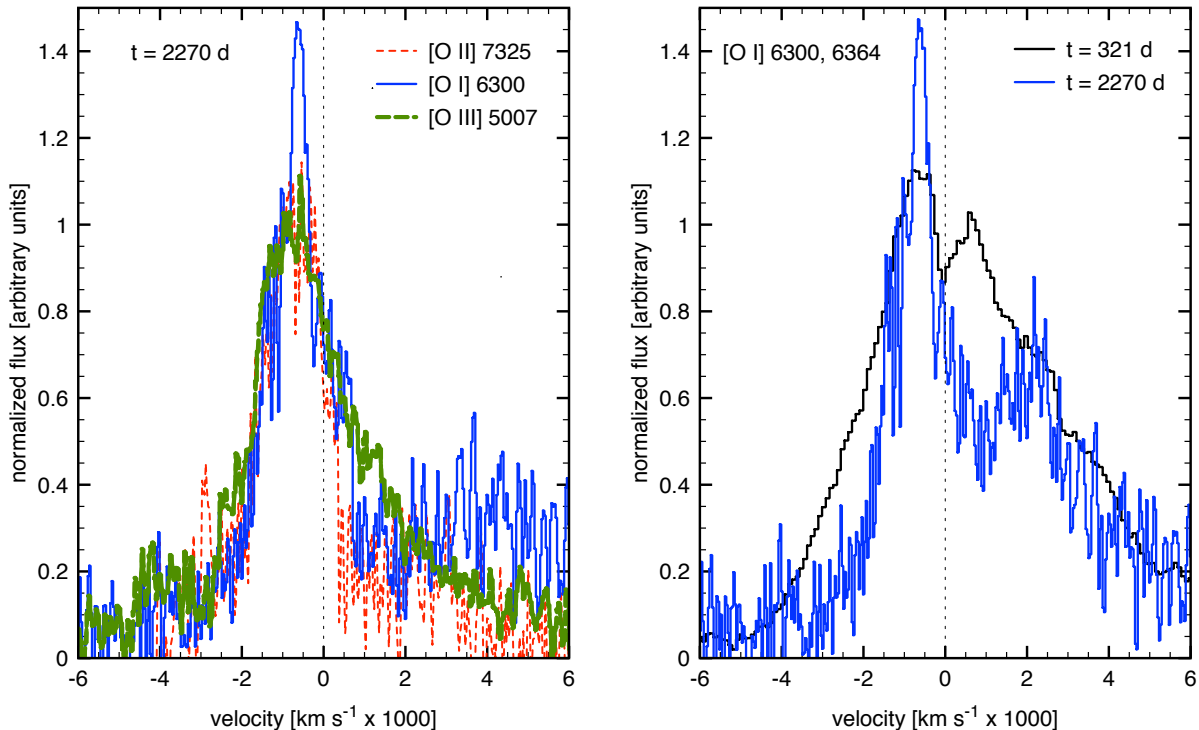


**Figure 2.** *Left:* Modified [O II], [O I], and [O III] emission line profiles of SN 2012au. Companion doublet lines [O I]  $\lambda$ 6364 and [O III]  $\lambda$ 4959 have been modeled and subtracted from the profiles, and the [O II]  $\lambda$  $\lambda$ 7319, 7330 blend has been treated as a single line with Doppler velocities with respect to 7325 Å. *Right:* Unmodified [O I] emission line profiles for days 321 and 2270.

No narrow ( $\text{FWHM} < 200 \text{ km s}^{-1}$ ) features are observed in the spectrum. Particular attention was made to possible emission in the region of  $\text{H}\alpha$ , which would be indicative of interaction with H-rich CSM. The 2D spectrum shows narrow emission lines of [O I] 6300, 6364, [N II] 6548, 6583, and  $\text{H}\alpha$  extended spatially across the slit but nothing conspicuous and specific to the SN location (Fig. 1, bottom). After careful subtraction of the local background we estimate an upper limit of  $\text{H}\alpha$  emission to be  $< 4.1 \times 10^{-17} \text{ erg s}^{-1} \text{ cm}^{-2}$ .

### 3.2. Emission line diagnostics

The emission line intensity ratios of our spectra can be used with atomic rates from CHIANTI (Del Zanna et al. 2015) to constrain properties of the ejecta. The intensity ratio  $\text{O I}/[\text{O II}]$  is a sensitive temperature diagnostic and the measured ratio of  $\approx 0.27$  indicates a temperature  $T \approx 5000 \text{ K}$ . However, this should be viewed as an average temperature of the  $\text{O}^+$  zone. Because the line profile of O I does not closely follow those of the other lines (section 3.1), some emission may originate from a different region of the ejecta and include cool gas that does not emit in the collisionally excited lines.

The  $[\text{O III}]/[\text{S III}]$  ratio reflects a higher temperature of the  $\text{O}^{++}/\text{S}^{++}$  zone. If we assume that  $(\text{S}^{++}/\text{S}) = (\text{O}^{++}/\text{O})$ , then the measured ratio of  $[\text{S III}]/[\text{O III}] =$

0.146 can be used in the expression

$$[\text{S III}]/[\text{O III}] = 5.98 \times [\text{S}/\text{O}] \times \exp(12800/T)$$

to give

$$\text{S}/\text{O} = 0.024 \times \exp(-12800/T).$$

The assumption of equal ionization fractions for S and O is plausible, but it potentially introduces an uncertainty of a factor of 2.

Notably, [S III]  $\lambda$ 9531 line emission is observed, but [S II]  $\lambda$  $\lambda$ 6717, 6731 is absent. This suggests electron densities above  $10^4 \text{ cm}^{-3}$ . Using the ratio of S/O from the equation above at  $10^4 \text{ K}$ , assuming  $(\text{S}^+/\text{S}) = (\text{O}^+/\text{O})$  in the singly ionized zone, and that  $\log T$  is at least 3.7, then the ratio of  $[\text{S II}]/[\text{O II}]$  as a function of density can be determined. Estimating the upper limit to emission centered around the [S II]  $\lambda$  $\lambda$ 6716,6731 lines to be  $\approx 0.2 \times I([\text{O II}])$ , we find that  $\log T = 3.8$  and  $\log n \gtrsim 6.0$ .

We thus conclude a sulfur to oxygen ratio  $\sim 0.01$  and a density of  $\log n \gtrsim 6.0$ . The high density is likely associated with significant clumping of ejecta, because a uniform sphere at that density with the radius  $R \sim 4.3 \times 10^{16} \text{ cm}$  given by the time since explosion and observed expansion velocity would produce far more than the observed luminosity. The line profiles of all the forbidden oxygen lines are roughly the same

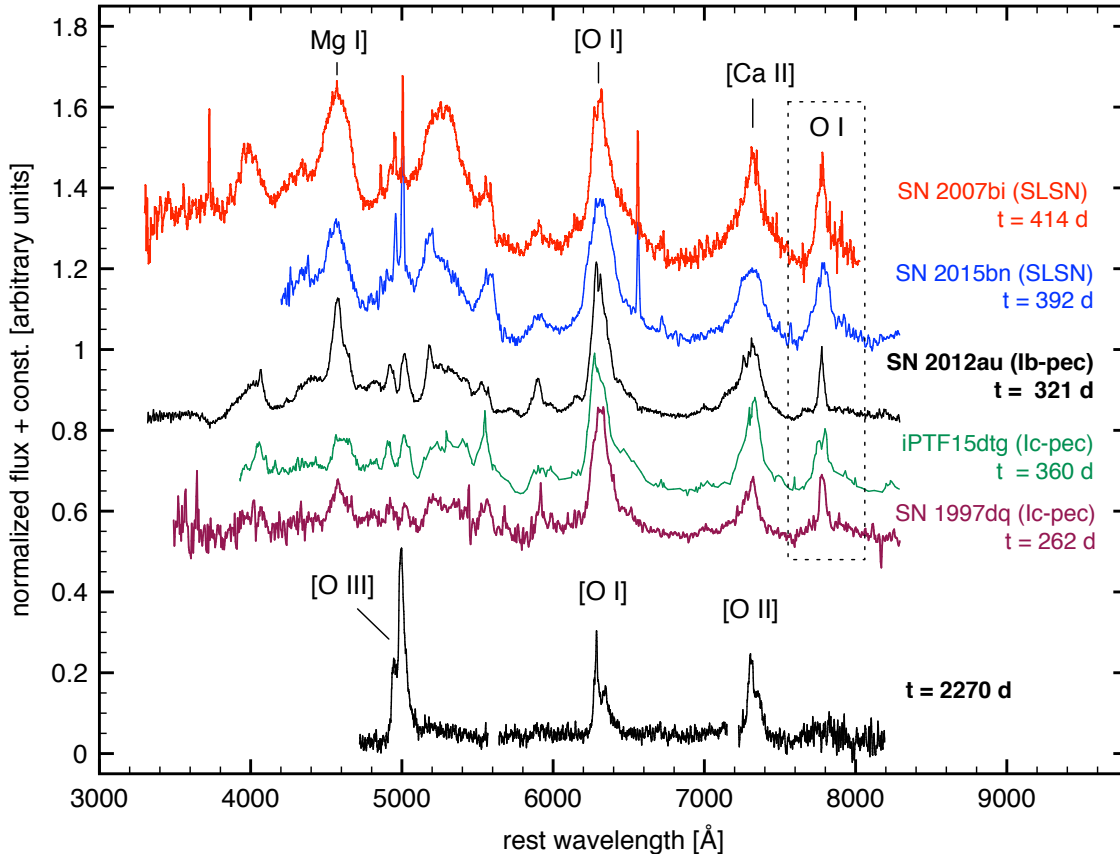


**Figure 3.** Earlier nebular spectrum ( $t \approx 1$  yr) of SN 2012au (Milisavljevic et al. 2013) compared to our  $t = 6.2$  yr spectrum. Also shown is a subset of related SLSNe (e.g., SNe 2007bi and 2015bn; Gal-Yam et al. 2009 and Nicholl et al. 2016), and SNe Ic (SN 1997dq and iPTF15dtg; Matheson et al. 2001 and Taddia et al. 2018). The O I  $\lambda 7774$  line, which is a defining feature of the related objects, has faded. All events may evolve to a similar late-time emission phase.

(Fig. 2), indicating that they are likely co-located, but with  $O^{++}$  associated with a lower density, higher temperature zone.

#### 4. DISCUSSION

Our  $t = 6.2$  yr spectrum of SN 2012au is markedly different from the last published spectrum at  $t \sim 1$  yr (Milisavljevic et al. 2013; Fig. 3). At that time SN 2012au exhibited [O I], [Ca II], and Mg I] emissions typical of stripped-envelope core-collapse SNe, and unusually strong emissions from Ca II H&K, Na I D, and O I 7774. It also showed persistent P-Cyg absorptions attributable in part to Fe II at  $2000 \text{ km s}^{-1}$ . None of these features are observed in the new spectrum, with the exception of [O I] that has a radically different emission line profile (Fig. 2) and the weakly detected O I.

Figure 3 also shows examples of objects that share late-time emission properties of SN 2012au. The recently reported optical spectrum of iPTF15dtg (Taddia et al. 2018) that we identify as a member of this grouping is included as well. Milisavljevic et al. (2013) noted that asymmetries between the emission line profiles of ions in

these objects are consistent with moderately aspherical explosions. They also highlighted the O I  $\lambda 7774$  line of width  $\approx 2000 \text{ km s}^{-1}$  as being indicative of a jetted explosion and a defining feature of these objects. Nicholl et al. (2016) later interpreted the O I feature to be the signature of heating of a shell by a central engine.

Below we discuss possible excitation mechanisms for the late-time spectrum of SN 2012au and utilize multi-wavelength data that further constrain properties of the ejecta and CSM.

##### 4.1. Radioactivity and SN-CSM interaction

Typically, late-time spectra of SNe I at stages reaching one year are still powered by radioactive  $^{56}\text{Co}$  in the  $^{56}\text{Ni} \rightarrow ^{56}\text{Co} \rightarrow ^{56}\text{Fe}$  decay chain. However, radioactivity is not a plausible heating source for the oxygen-rich ejecta at  $t = 6.2$  yr considering  $\approx 0.3 M_{\odot}$  of  $^{56}\text{Ni}$  was produced in SN 2012au (Milisavljevic et al. 2013; Takaki et al. 2013) and  $^{56}\text{Co}$  has a half-life of 77.3 days (Alburger et al. 1989). Furthermore, radioactivity is typically associated with neutral and singly ionized lines

(see, e.g., Matheson et al. 2001), and yet our 6.2 yr spectrum exhibits a larger range of ionization levels.

SN–CSM interaction is the most common late-time emission mechanism for objects observed  $> 3$  yr post-explosion (see Milisavljevic et al. 2012 and Chevalier & Fransson 2017 and references therein). Optical emission principally originates from a reverse shock that propagates upstream into outward expanding ejecta that gets heated and ionized. Such late-time detections all have clear signatures of interaction with an H-rich CSM including development of narrow emission lines and/or high velocity H-rich ejecta (Milisavljevic & Fesen 2017; Fig. 4). SNe Ib,c examples include SN 2001em (Chugai & Chevalier 2006), SN 2014C (Milisavljevic et al. 2015), and SN 2004dk (Mauerhan et al. 2018). A few SLSNe-I have exhibited hydrogen emission several hundred days after explosion (Yan et al. 2017). This contrasts with SN 2012au, which shows no spectral features indicative of SN–CSM interaction.

If SN 2012au was indeed interacting with H-rich material, then H Balmer line emission would be expected. Certain H-rich CSM distributions could potentially inhibit optical emission at the time of observation, but such configurations are considered to be unlikely. It is also possible that SN 2012au is interacting with an H-poor environment. This scenario has been discussed in the context of SLSNe-I (Chatzopoulos & Wheeler 2012), but the detailed spectroscopic properties predicted for helium/carbon/oxygen-rich CSM interaction at these extremely late epochs is poorly explored.

#### 4.2. Pulsar Wind Nebula

Another late-time emission mechanism is pulsar interaction with expanding SN gas. A PWN is generated by the spin-down power of a central pulsar. In this scenario, photoionization of the inner regions of the expanding shell of ejecta can be the dominant source of optical line emission, especially at early times ( $< 10$  yr) when the expanding ejecta absorb much of the PWN-emitting ionizing radiation.

The Chevalier & Fransson (1992) model is based on the young Crab Nebula and has been widely used for pulsar and magnetar nebulae (e.g., Kasen & Bildsten 2010). The freely expanding SN density profile is approximated by an inner, flatter power law density profile surrounded by a steeper one. The inner profile has index  $m = 1$  and the outer  $n = 9$  (Chevalier & Soker 1989; Matzner & McKee 1999). For the SN 2012au parameters  $E_k \sim 10^{52}$  erg and  $M_{ej} \approx 4 M_\odot$ , the transition between these power laws occurs at  $18,000$  km  $s^{-1}$ . Thus the SN 2012au PWN is well within the inner, flatter region of the freely expanding gas. From equ. (2.11) of Cheva-

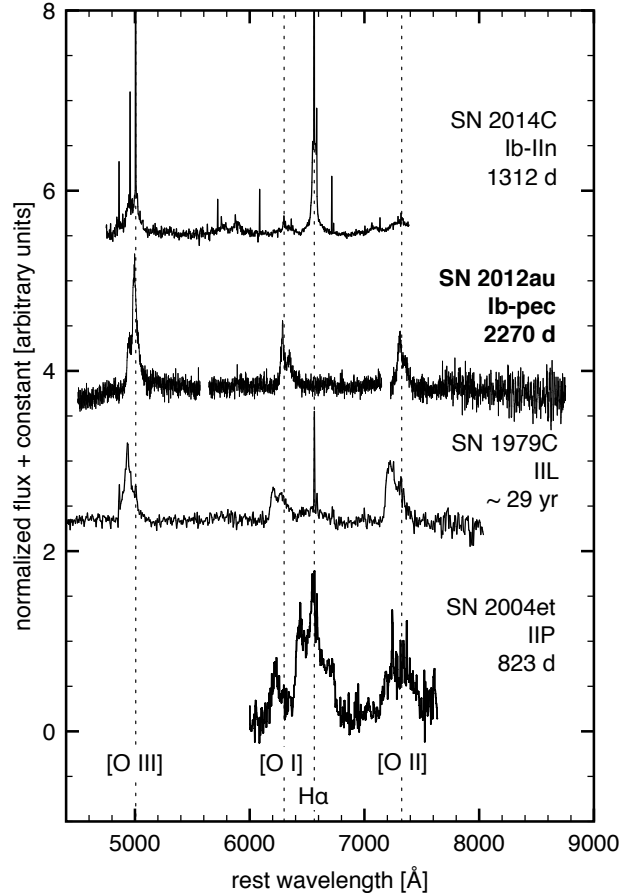


**Figure 4.** With the exception of SN 2012au, optical spectra of SNe observed at epochs  $t > 3$  yr show hydrogen lines and evidence for SN–CSM interaction. Examples shown here are SN 2014C (Mauerhan et al. 2018), SN 1979C (Milisavljevic et al. 2009), and SN 2004et (Kotak et al. 2009).

lier & Fransson (1992), the velocity  $V$  of the PWN is

$$V = 289 \dot{E}_{39}^{0.25} E_{k51}^{0.25} M_{ej1}^{-0.5} t_{yr}^{0.25} \text{ km s}^{-1}, \quad (1)$$

where  $\dot{E}_{39}$  is in units of  $10^{39}$  erg  $s^{-1}$ ,  $E_{k51}$  in  $10^{51}$  ergs,  $M_{ej1}$  in  $10 M_\odot$ , and  $t_{yr}$  in years. With  $V = 2300$  km  $s^{-1}$  (assuming the emission is coming from close to the shell),  $E_{k51} = 10$ ,  $M_{ej1} = 0.4$ , and  $t_{yr} = 6.2$ , we have  $\dot{E} = 10^{40}$  erg  $s^{-1}$ . The Crab pulsar currently has  $\dot{E} \approx 4 \times 10^{38}$  erg  $s^{-1}$  (e.g., Condon & Ransom 2016) and extrapolating back with constant braking index gives an initial  $\dot{E} \approx 4 \times 10^{39}$  erg  $s^{-1}$ , quite close to what is needed for SN 2012au. The Crab magnetic field is  $B \approx 4 \times 10^{12}$  G (e.g., Condon & Ransom 2016), well below the magnetar field  $B > 10^{14}$  G. Hence, the pulsar in SN 2012au is potentially more Crab-like than magnetar-like.

The Chevalier & Fransson (1992) model includes line estimates for an O zone. It predicts an [O III] luminosity at 1500 days to be  $0.46 \times 10^{38}$  erg  $s^{-1}$ , which is

close to the  $1.4 \times 10^{38} \text{ erg s}^{-1}$  observed in SN 2012au. [O I] is weak because a thermal instability cools the gas, but somewhat different parameters could increase [O I]. [O II] is weak because of low temperature and high density, but that could also change. The high energy of SN 2012au should result in a considerably lower density than the PWN is moving into than in the Crab.

Chevalier & Fransson (1992) assumed that the swept up shell would be broken up by instabilities so the ionizing radiation from the PWN photoionizes freely expanding gas ahead of the shock front. In that case, there are different layers of ionized and neutral O in the O zone. However, the similar line profiles for [O I], [O II], and [O III] (Fig. 2) do not support this picture.

A radiative shock wave driven into the freely expanding ejecta by the PWN is another possible excitation mechanism. However, the efficiency of this process is low,  $L \sim 0.015 \times \dot{E}$ . Also, one would expect the characteristic boxy line profile for shell emission, which is not observed.

The most likely scenario seems to be photoionization of O zone gas that has been shocked by the high pressure PWN and subjected to instabilities. In the Crab, the photoionization is of the H/He zone. Both SN 2012au and the Crab show fairly centrally peaked line profiles, as would be expected if Rayleigh-Taylor instabilities mix gas to the central region. Blondin & Chevalier (2017) performed a simulation of this process (see Fig. 3 of that paper). Dense gas is in both Rayleigh-Taylor fingers and an outer shocked shell. Photoionization layers are anticipated, but on a small scale, so the line profiles of different ions will be similar. The compression in the PWN-driven shock also leads to the high density deduced from line diagnostics (section 3.2).

A prediction of the above pulsar model is broadening of the emission lines with time because of the acceleration of the pulsar bubble. Following Chevalier & Fransson (1992), one would expect roughly steady pulsar power leading to  $R \propto t^{1.25}$  for the swept up shell or velocity  $V \propto t^{0.25}$ . Specifically for SN 2012au, we anticipate

$$\delta V/V = 0.25 \delta t/t = 0.25(1 \text{ yr}/6.2 \text{ yr}) = 0.04$$

in one year, or a rate of increase in the emission line velocity width of  $\approx 4\% \text{ yr}^{-1}$ .

In the above model, it is assumed that the initial pulsar spindown timescale is much greater than the age. If the spindown timescale is much less than the age, the pulsar input occurs early and the shell tends to a constant velocity; the shell comoves with the freely expanding gas and  $V = R/t$ . The kinetic energy of the shell depends on the mass, which can be found from the

freely expanding density profile, and velocity  $V$ , yielding  $E_k = 2.5 \times 10^{48} \text{ ergs}$ . The energy of freely expanding gas is  $1.3 \times 10^{48} \text{ ergs}$ , which implies that the initial rotational energy of the pulsar,  $E_0$ , was  $1.3 \times 10^{48} \text{ ergs}$ , corresponding to a rotation period of 0.13 s. This is longer than the ms periods found in the magnetar models for SLSNe and is due to the  $V^4$  dependence of  $E_k$  (eqn. (1)); line widths in the magnetar model approach  $\sim 12,000 \text{ km s}^{-1}$  and remain constant.

We favor the long spindown model because it implies a current pulsar power that is roughly consistent with that needed to produce the observed luminosity. A prediction of this model is increasing PWN velocities, as opposed to constant velocities in the short spindown case. Deceleration is not expected in a PWN model.

## 5. X-RAY EMISSION FROM THE PWN

We considered the viability of detecting X-rays from the candidate PWN. Assuming a dipole model for the central source, with a spin period of 1 ms, the spindown luminosity is given as

$$L_p \approx 2 \times 10^{42} B_{14}^2 (t/\text{yr})^{-2} \text{ erg s}^{-1},$$

where  $B_{14}$  is the magnetic field in units of  $10^{14} \text{ G}$ . At the time of our *CXO* observation ( $t = 2325 \text{ d}$ ),  $L_p \lesssim 10^{41} \text{ erg s}^{-1}$ . If only 1% of that is converted into X-rays, the expected luminosity of the central source is  $\sim 10^{39} \text{ erg s}^{-1}$ . This would be the most favorable situation, and a less energetic PWN would have a lower luminosity.

We can estimate the optical depth to 1 keV X-rays as

$$\tau = (\sigma/16 m_p) \times 3/(4\pi) * M_{ej}/(v_{ej}t)^2,$$

where  $\sigma$  is the cross section for 1 keV X-rays,  $m_p$  is the proton mass,  $v_{ej}$  is the initial ejecta velocity, and  $t$  is the age in years. Assuming a cross section of  $10^{-19} \text{ cm}^2$ , appropriate for oxygen-rich ejecta, and  $v_{ej}$  upwards of  $\sim 3 \times 10^4 \text{ km s}^{-1}$ , the optical depth to 1 keV X-rays is  $\gg 1$ . Thus, the *CXO* non-detection is consistent with our estimate that the candidate PWN of SN 2012au is presently optically thick to 1 keV X-rays.

Notably, SN-CSM interaction (see Chevalier & Fransson 2017) is a possible alternative source of late-time X-ray emission. However, adopting parameters estimated in Kamble et al. (2014) (progenitor mass loss rate  $\dot{M} \approx 4 \times 10^{-6} M_\odot \text{ yr}^{-1}$ , with a wind speed of  $v_w = 1000 \text{ km s}^{-1}$  extending out to a radius of at least  $10^{17} \text{ cm}$ ), the expected thermal X-ray emission associated SN-CSM interaction would only be  $\lesssim 10^{32} \text{ erg s}^{-1}$ . This translates to a 0.5–10 keV X-ray flux of  $\sim 10^{-20} \text{ erg cm}^{-2} \text{ s}^{-1}$ , which is well below our detection limit.

## 6. CONCLUSIONS

We have presented optical and X-ray observations of the energetic, slow-evolving, Type Ib SN 2012au obtained  $> 6$  yr post-explosion that provide direct evidence of a newly-formed PWN exciting O-rich ejecta. Our findings support the notion that SN 2012au and a subset of SLSNe, GRB-SNe, and SNe Ib/c have been relatedly influenced by magnetized compact objects on a wide range of energy scales. It remains unclear what key aspects of the progenitor systems unite these SNe that span absolute magnitudes of  $-22 < M_B < -17$ .

We anticipate that, like SN 2012au, SNe harboring influential pulsar/magnetar wind nebulae will evolve into a late-time phase dominated by forbidden oxygen transitions. Furthermore, we predict that optical emission line widths should remain constant or broaden upwards of a few per cent per year due to acceleration of ejecta by the pulsar/magnetar bubble. In the specific case of SN 2012au, we estimate velocity broadening at the rate of  $4\% \text{ yr}^{-1}$ . Measurements are potentially achievable with return visits from 8-10-m class telescopes using

$R \gtrsim 10000$  spectroscopy over the next several years, although best opportunities for distant events await the arrival of next-generation Extremely Large Telescopes.

We thank the referee for a very helpful reading of the paper and suggestions that significantly improved its content and presentation. This paper includes data gathered with the 6.5 meter Magellan Telescopes located at Las Campanas Observatory, Chile. D.J.P. acknowledges support from NASA Contract NAS8-03060. We thank the *Chandra X-ray Observatory* for the Director's Discretionary Time which made possible the X-ray observations cited in this paper. Data for SNe 1997dq 2007bi, and 2015bn were retrieved from the Weizmann interactive supernova data repository (<http://wiserep.weizmann.ac.il>). J. Mauerhan kindly shared spectra of SN 2014C. R.A.C. acknowledges support from NSF grant AST-1814910.

*Facilities:* Magellan: Baade (IMACS), CXO

## REFERENCES

- Alburger, D. E., Warburton, E. K., & Tao, Z. 1989, *Phys. Rev. C*, 40, 2789
- Angus, C. R., Levan, A. J., Perley, D. A., et al. 2016, *MNRAS*, 458, 84
- Blondin, J. M., & Chevalier, R. A. 2017, *ApJ*, 845, 139
- Chatzopoulos, E., & Wheeler, J. C. 2012, *ApJ*, 760, 154
- Chevalier, R. A., & Fransson, C. 1992, *ApJ*, 395, 540
- . 2017, *Thermal and Non-thermal Emission from Circumstellar Interaction*, ed. A. W. Alsabti & P. Murdin, 875
- Chevalier, R. A., & Irwin, C. M. 2011, *ApJL*, 729, L6
- Chevalier, R. A., & Soker, N. 1989, *ApJ*, 341, 867
- Chugai, N. N., & Chevalier, R. A. 2006, *ApJ*, 641, 1051
- Condon, J. J., & Ransom, S. M. 2016, *Essential Radio Astronomy*, Princeton, NJ: Princeton University Press
- Coppejans, D. L., Margutti, R., Guidorzi, C., et al. 2018, *ApJ*, 856, 56
- Del Zanna, G., Dere, K. P., Young, P. R., Landi, E., & Mason, H. E. 2015, *A&A*, 582, A56
- Dressler, A., Bigelow, B., Hare, T., et al. 2011, *PASP*, 123, 288
- Eftekhari, T., Berger, E., Williams, P. K. G., & Blanchard, P. K. 2018, *ApJ*, 860, 73
- Gal-Yam, A., Mazzali, P., Ofek, E. O., et al. 2009, *Nature*, 462, 624
- Greiner, J., Mazzali, P. A., Kann, D. A., et al. 2015, *Nature*, 523, 189
- Hamuy, M., Maza, J., Pinto, P. A., et al. 2002, *AJ*, 124, 417
- Inserra, C., Smartt, S. J., Jerkstrand, A., et al. 2013, *ApJ*, 770, 128
- Kalberla, P. M. W., Burton, W. B., Hartmann, D., et al. 2005, *A&A*, 440, 775
- Kamble, A., Soderberg, A. M., Chomiuk, L., et al. 2014, *ApJ*, 797, 2
- Kasen, D., & Bildsten, L. 2010, *ApJ*, 717, 245
- Kotak, R., Meikle, W. P. S., Farrah, D., et al. 2009, *ApJ*, 704, 306
- Lunnan, R., Chornock, R., Berger, E., et al. 2014, *ApJ*, 787, 138
- . 2018, *ApJ*, 852, 81
- MacFadyen, A. I., & Woosley, S. E. 1999, *ApJ*, 524, 262
- Margutti, R., Chornock, R., Metzger, B. D., et al. 2017, *arXiv:1704.05865*
- Matheson, T., Filippenko, A. V., Li, W., Leonard, D. C., & Shields, J. C. 2001, *AJ*, 121, 1648
- Matzner, C. D., & McKee, C. F. 1999, *ApJ*, 510, 379
- Mauerhan, J. C., Filippenko, A. V., Zheng, W., et al. 2018, *MNRAS*, 478, 5050
- Mazzali, P. A., McFadyen, A. I., Woosley, S. E., Pian, E., & Tanaka, M. 2014, *MNRAS*, 443, 67
- Metzger, B. D., Berger, E., & Margalit, B. 2017, *ApJ*, 841, 14
- Metzger, B. D., Giannios, D., Thompson, T. A., Bucciantini, N., & Quataert, E. 2011, *MNRAS*, 413, 2031



- Metzger, B. D., Margalit, B., Kasen, D., & Quataert, E. 2015, *MNRAS*, 454, 3311
- Milisavljevic, D., & Fesen, R. A. 2017, *The Supernova — Supernova Remnant Connection*, ed. A. W. Alsabti & P. Murdin, 2211
- Milisavljevic, D., Fesen, R. A., Chevalier, R. A., et al. 2012, *ApJ*, 751, 25
- Milisavljevic, D., Fesen, R. A., Kirshner, R. P., & Challis, P. 2009, *ApJ*, 692, 839
- Milisavljevic, D., & Margutti, R. 2018, *SSRv*, 214, 68
- Milisavljevic, D., Soderberg, A. M., Margutti, R., et al. 2013, *ApJL*, 770, L38
- Milisavljevic, D., Margutti, R., Kamble, A., et al. 2015, *ApJ*, 815, 120
- Nicholl, M., Berger, E., Blanchard, P. K., Gomez, S., & Chornock, R. 2018, *arXiv:1808.00510*
- Nicholl, M., Williams, P. K. G., Berger, E., et al. 2017, *ApJ*, 843, 84
- Nicholl, M., Berger, E., Margutti, R., et al. 2016, *ApJL*, 828, L18
- Nicholl, M., Smartt, S. J., Jerkstrand, A., et al. 2013, *Nature*, 502, 346
- Pastorello, A., Smartt, S. J., Botticella, M. T., et al. 2010, *ApJL*, 724, L16
- Pian, E., & Mazzali, P. A. 2017, *Hydrogen-Poor Core-Collapse Supernovae*, ed. A. W. Alsabti & P. Murdin, 277
- Taddia, F., Sollerman, J., Fremling, C., et al. 2018, *ArXiv e-prints*, *arXiv:1806.10000*
- Takaki, K., Kawabata, K. S., Yamanaka, M., et al. 2013, *ApJL*, 772, L17
- Theureau, G., Hanski, M. O., Coudreau, N., Hallet, N., & Martin, J.-M. 2007, *A&A*, 465, 71
- Thompson, T. A., Chang, P., & Quataert, E. 2004, *ApJ*, 611, 380
- van Dokkum, P. G. 2001, *PASP*, 113, 1420
- Woosley, S. E., & Heger, A. 2012, *ApJ*, 752, 32
- Yan, L., Lunnan, R., Perley, D. A., et al. 2017, *ApJ*, 848, 6